Carbon 149 (2019) 63–70

Contents lists available at ScienceDirect

Carbon

journal homepage: www.elsevier.com/locate/carbon

A tactile sensing textile with bending-independent pressure perception and spatial acuity

Jue Deng [a,1], Wen Zhuang [a,1], Luke Bao [a], Xiaoying Wu [a], Jingbo Gao [b], Bingjie Wang [a], Xuemei Sun [a,*], Huisheng Peng [a,**]

[a] State Key Laboratory of Molecular Engineering of Polymers, Department of Macromolecular Science, Laboratory of Advanced Materials, Fudan University, Shanghai, 200438, China
[b] State Key Laboratory of ASIC and System, School of Microelectronics, Fudan University, Shanghai, 201203, China

ARTICLE INFO

Article history:
Received 28 January 2019
Received in revised form
23 March 2019
Accepted 6 April 2019
Available online 12 April 2019

ABSTRACT

The integration of tactile sensor into textile is a promising strategy to address the requirements of light weight, flexibility, compilability and breathability in the next-generation wearable electronics. However, achieving reliable and accurate tactile perception remains difficult for sensing textiles as the quantitative measurements are interfered by geometric deformations and the spatial resolutions are disturbed by the adjacent pixels. Here, we overcome the above challenges by designing helically swollen architecture in core-sheath fibers for tactile sensing textiles (TSTs) that show bending-independent pressure perception and spatial acuity. The building fibers can accurately detect pressure under different radii of curvature and recognize touching positions, so the TSTs can precisely map the surface pressure distribution during deformation. As a demonstration, they are integrated into a smart glove as an accurate tactile monitor and human-machine interface. It will help to improve the reliability and accuracy in the practical development of wearable electronics and smart textiles.

1. Introduction

In the burgeoning field of wearable electronics, pressure sensors have attracted increasing interests due to the promising function of transducing mechanical stimuli into processible electrical signals for mobile healthcare monitoring [1–4], soft robotics [5,6] and human–machine interfaces [7–10]. Textile pressure sensor is a promising candidate for the next-generation sensing platform since it can be easily incorporated into modern garments in a breathable, comfortable and conformable way [11–15]. Recently, various high-performance textile pressure sensors were developed based on different mechanisms, such as piezoresistive [15–17], capacitive [18–20] and piezoelectric [21,22].

Despite the improvements in the sensitivity and response time of pressure sensors [3,23–25], reliable and accurate pressure detection is still a challenge for textile sensors in real-time measurement. On the one hand, quantitative measurement of pressure stress would be distorted once bending stress is applied simultaneously. Given the curvilinear surface of human body and the waved structure in woven textiles, the functional fiber unit in textile-based sensor is frequently exposed to vertical pressure stress and bending stress simultaneously [7,26]. Previous textile pressure sensors can hardly distinguish two types of stresses [20,27] as both bending and pressing deformations caused the similar variation of the contact areas [28] or distance [29] between two electrodes in conventional pressure sensors, and the resulted electric responses were in the same magnitude. On the other hand, the spatial resolution of textile-based pressure sensor was limited as they can hardly differentiate the pressure location precisely. Based on the geometrical advantage of braided structure of textiles, a strategy of cross-stacking the fiber units perpendicularly had been widely adapted for mapping the pressure distribution [23,30]. Although the sensory pixels formed by the overlapped area in each row and column can achieve regional mapping of external forces in the whole matrix, the spatial resolution in such configuration was limited by the cross-talk among adjacent pixels due to the interlaced nature of cross-stacked network [8,31]. Therefore, it is difficult to realize the reliability and accuracy of quantitative

* Corresponding author.
** Corresponding author.
E-mail addresses: sunxm@fudan.edu.cn (X. Sun), penghs@fudan.edu.cn (H. Peng).
[1] These authors contributed equally to this work.

https://doi.org/10.1016/j.carbon.2019.04.019

measurement and spatial resolution in tactile perception.

Here, we report a tactile sensing textile (TST) with bending-independent pressure perception and spatial acuity assembled from core-sheath sensing fibers to overcome the above challenges. By designing a novel helically swollen architecture in the substrate, the microscopic structure and conductive path in a core-sheath fiber keep the same configuration regardless of bending stress. Therefore, the TST showed identical pressure sensitivity under different radii of curvature. The robust bending-independent responses of TST were not disturbed by the direction of applied force and frequency. Furthermore, benefitting from the core-sheath structure, touching position along a single fiber can be accurately recognized to avoid the cross-talk among adjacent pixels in conventional textile sensors. Combining quantitative measurement with improved spatial acuity, the resulting TST can precisely map the pressure distribution, even in an extremely folded shape. As a demonstration, the TSTs were integrated into smart gloves to detect physical contacts under different gesticulations, and they served as an accurate tactile monitor and wirelessly control mobile phone for efficient human-machine interface.

2. Experimental section

2.1. Fabrication of carbon nanotube (CNT)/polyurethane (PU) sheath electrode

The aligned CNT sheets were continuously drawn from spinnable CNT arrays and spirally wound onto a polytetra fluoroethylene (PTFE) fiber substrate with a diameter of 1 mm. The helical angle of aligned CNT layer on the fiber substrate was 45° and the thickness of CNT layers can be well controlled by the width of CNT sheets and the number of winding times. Polyurethane (PU) solution was prepared by dissolving PU powders (24 g, Huntsman) in DMF (40 mL) under mechanical stirring at 80 °C for 1.5 h. The prepared PU solution was sonicated to remove the bubbles. The CNT-wrapped fiber was then immersed into the PU solution at a speed of 200 mm/min, stayed for 3 s and pulled out at 30 mm/min. After the dip-coating process, the composite fiber was immediately immersed in a DMF/deionized water mixture (1/1, v/v) for 5 min. The solidified sheath electrode was fabricated by carefully pulling out of the PTFE fiber (Fig S1). The CNT layer was completely removed from the PTFE substrate and covered the inner surface of PU sheath homogeneously. The resulting CNT/PU sheath electrode showed an average thickness of 120 μm. The inner and outer diameter of sheath electrode is 1000 and 1250 μm, respectively. The PU layer in the sheath electrode can also serve as a protection layer for the whole device and physically block the interaction between device components and external environment.

2.2. Preparation of copper/shape memory polymer (SMP) core electrode

The core electrode consisted of an SMP fiber and a twisted copper wire. SMP fiber (SMP Technologies Inc. MP-4510) was prepared by mixing two components (1/1, v/v) for 20 s, followed by injecting SMP solution into a plastic tube with an inner diameter of 1 mm, curing in an oven (temperature of 70 °C) for 2 h, and peeling off the plastic tube. The resulting SMP fiber showed an initial diameter of 1 mm. Then the SMP fiber was stretched to about twice of the initial length at 80 °C and cooled down to room temperature, forming a temporary diameter of 700 μm. A washed copper wire with a diameter of 50 μm was then spirally wound onto the pre-stretched SMP fiber with helical angle of 60°, 65°, 70° or 75° (Fig S2). The screw pitches decreased with the increasing helical angles from 60° to 75° and the smaller screw pitches provided larger geometry constraints to pre-stretched SMP fibers.

2.3. Fabrication of sensing fiber and sensing textile

The sensing fiber was fabricated by inserting the pre-stretched core electrode (diameter: 700 μm) into sheath electrode (inner diameter: 1000 μm), followed by gradually heating the core electrode to undergo linear shrink and generate helical swollen architectures (Fig S3 and S4). The core electrode was spirally bulked with a fixed pitch of 790, 640, 530 or 400 μm. The diameter of sensing fibers can be easily tuned by changing the template fiber substrate (Fig S5). Sensing fibers were woven with commercial yarns into sensing textiles and smart gloves for further applications by various textile techniques including commercial sewing machine (Fig S6). In both sensing fiber and textile, copper wire with an polymer encapsulating layer was used to connect the devices into external circuit and can also be woven into the fabrics and gloves (Fig S7).

3. Results and discussion

The concept of TST is shown in Fig. 1a. The sensing fibers, serving as warps or wefts, were plain woven with commercial yarns into the TST. The microscopic structure and conductive path of sensing fibers under flat (i) and bent states (ii) are showed in the enlarged illustrations. A sensing fiber consists of a carbon nanotube (CNT)/polyurethane (PU) sheath electrode and a copper/shape memory polymer (SMP) core electrode (Fig S1). The pressure response of prepared core-sheath fiber was based on piezoresistive mechanism. When the fiber is subject to an increasing pressure, the connection between the core and sheath electrodes is enhanced so that the resultant conductance increases. For the sheath electrode, aligned CNT sheets were uniformly covered on the inner surface of PU tubes (Fig. 1b and S1). Here, porous CNT sheets with high surface areas exhibits large variation in contact resistance under pressure, and robust and reversible mechanical properties with the help of composited PU. In addition, the resistance of sheath electrode can be well controlled by the thickness of CNT sheets [32,33] (Fig S8). A 200% pre-stretched SMP fiber helically wound with a copper wire was inserted into the sheath electrode (Fig S1), followed by gradually recovering the shape of SMP fiber to make a sensing fiber.

Three-dimensional X-ray micro-CT and scanning electron macroscopy (SEM) were used to characterize the configuration of sensing fibers. Due to the geometry constraint of copper wire, the pre-stretched SMP fibers were not able to completely recover to their original cylinder shapes but resulted in a helical swollen architecture (Fig. 1c, S3 and S4). The copper wire was tightly fastened on the surface of SMP fibers with a uniform spring shape after shape recovery. Through changing the screw pitch of helically wrapped copper wire on pre-stretched SMP, the extent of swollen architecture can be manipulated. In this case, the distance and contact areas between the CNT layer and copper wire can also be precisely controlled. Because the helical swollen architectures of SMP functioned as the separator, the core-sheath fibers showed the same microscopic configuration and conductive circuit regardless of the curvature in bent and wrinkled shapes, while conductive paths and contact areas between the CNT layer and the copper wire changed once pressure was loaded in the radial direction (Fig. 1a and Supporting Movie 1). The core and sheath electrodes were assembled into a fiber (Fig. 1d), and the as-prepared fiber showed

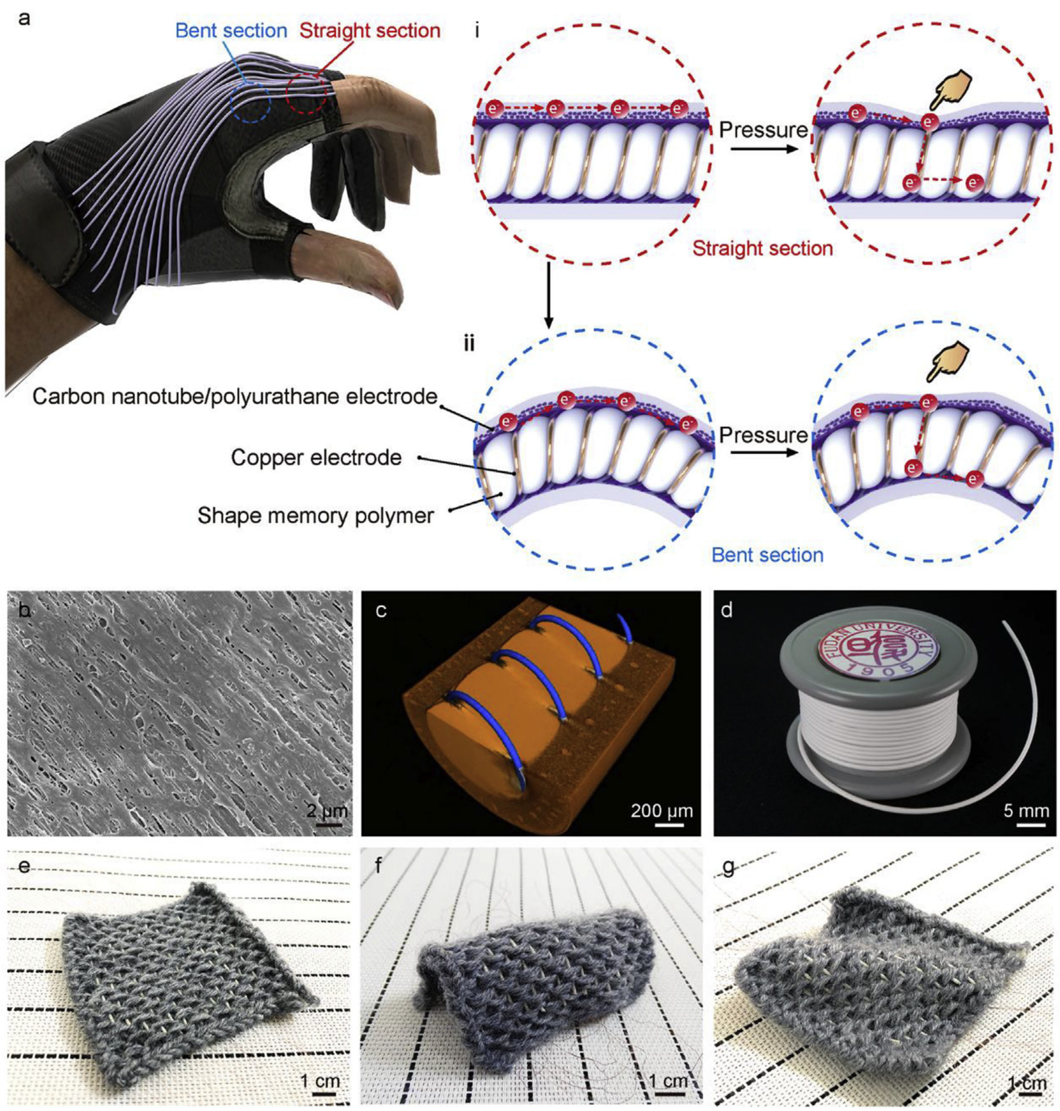

Fig. 1. | **Schematic illustration and structure of the tactile sensing textile (TST). a**, Illustrations and conceptual design of bending-independent TST. The conductive paths of straight (i) and bent (ii) sections are shown in the enlarged illustrations. **b**, SEM images of aligned CNT layer on the inner surface of a PU tube. **c**, Three-dimensional X-ray micro-CT image of bending-independent pressure-sensing fibers with a half of CNT/PU electrode and SMP fiber. **d**, Optical image of bending-independent pressure-sensing fibers. **e-g**, Optical images of TST in flat (**e**), bent (**f**) and wrinkled (**g**) shapes.

Young's modulus of ~500 MPa (Fig S9) similar with the other commercial yarns [34], which facilitate them to be woven into the TST (Fig. 1e). Thanks to the high flexibility of the building sensing fiber, the resulting TST can also be fixed into bent or wrinkled shapes (Fig. 1f and g), which is beneficial to conformally attach to the curvilinear human skin for accurate detections.

Supplementary video related to this article can be found at https://doi.org/10.1016/j.carbon.2019.04.019.

Minimizing the output difference between flat and bent devices is the key factor for accurately measuring the applied pressure. The microscopic structure of copper/SMP core electrode played an important role for the bending independence. With the increasing helical angles of copper wires from 60° to 65°, 70° and 75°, the pre-stretched SMP fibers were intertwined with denser copper wires. After shape recovery, helical swollen configurations generated and therefore created physical gaps between copper wire and CNT layer. The denser copper wires provided severer geometry constraints to pre-stretched SMP fibers, resulting in larger gaps between core and sheath electrodes. The resulting screw pitches of copper wires were 790, 640, 530 and 400 μm, respectively, and the gaps between copper wires and CNT layers were 0, 5, 15 and 30 μm, respectively, with the increasing helical angles from 60° to 65°, 70° and 75°. For the sensing fibers with 790, 640 and 530 μm screw pitches, the electrical resistances decreased severely under bending states (Fig. 2a). In contrast, when copper wire was wrapped on SMP fiber with 400 μm screw pitch at 75° helical angle, the devices possessed extremely stable electrical resistances during the bending test and it exhibited negligible variations up to the curvature of $2\,cm^{-1}$, which is larger than that of bent finger joints ($0.7\,cm^{-1}$) [35]. Further diminishing screw pitch requiring enhancement of helical angle generally caused the break of copper wires during preparation. Therefore, the core electrode with 400-μm-screw-pitch helical copper wire was chosen for the sensing fiber in further investigations.

The pressure sensitivity of sensing fibers was further measured under different curvatures. The CNT/PU electrode played an important role on the pressure sensitivity and the thickness of the PU layer was optimized. The thickness of PU layer can be controlled

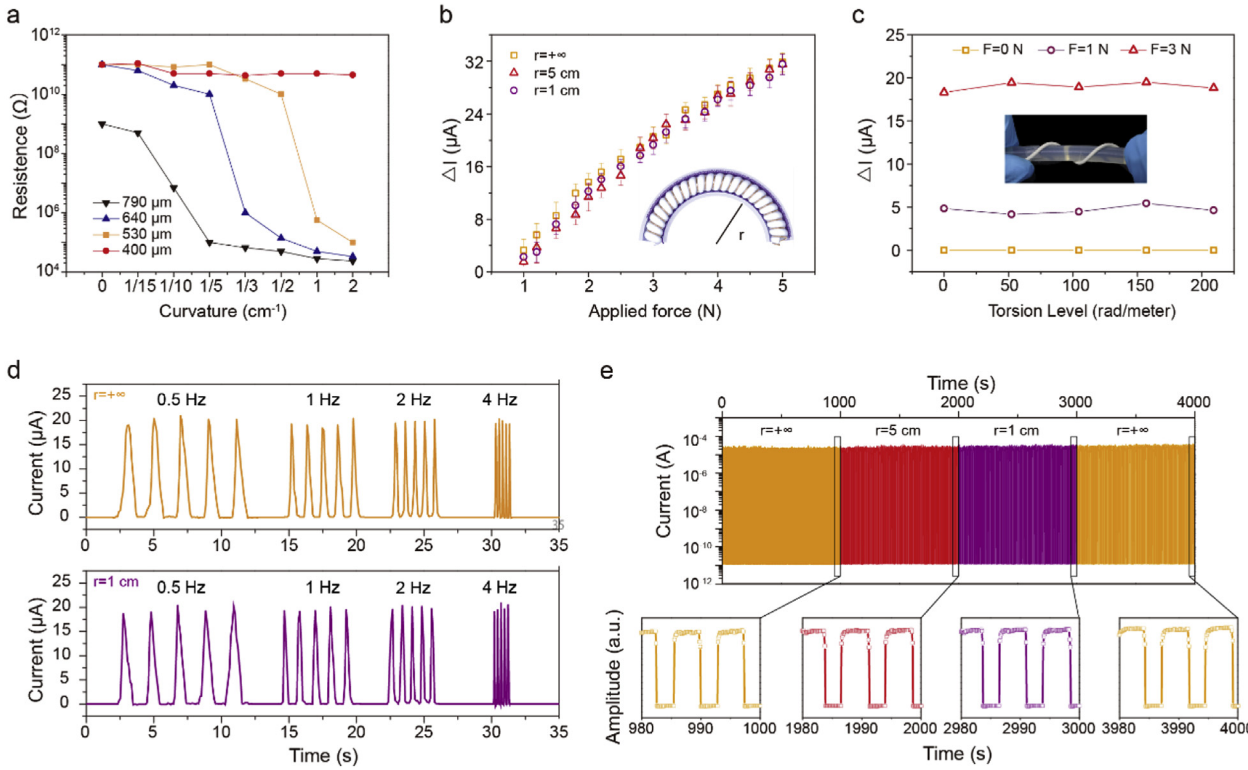

Fig. 2. | **Bending-independent pressure perception of TST. a**, Dependence of electrical resistance on curvature for helical copper wires with different screw pitches in core electrode. **b**, Dependence of current change on applied force for pressure-sensing fiber under different curvatures at the same touching point. **c**, Dependence of current change on applied force for pressure-sensing fiber under different torsion levels at the same touching point. Inset: Optical image of the sensing fiber wrapped around a rod at a fixed angle. **d**, Output currents in response to applied forces with different frequencies for pressure-sensing fiber with different curvatures. Frequencies of the applied force are 0.5, 1, 2 and 4 Hz **e**, Cyclic test of pressure-sensing fiber at different curvatures. The enlarged plots show the detailed current change for different curvatures. The testing voltage is 1 V in **b-e**, and the applied force is 3 N in **c-e**.

by the dip-coating speed (Fig S10). With the increasing thickness of PU layer, the sensitivity of sensing fibers obviously decreased due to the lower efficiency of stress transmission and smaller deformation under stress. On the other hand, the tubular shape was easy to collapse if the thickness was too thin. The optimized thickness of PU tube was 120 μm.

When pressure was applied to as-prepared sensing fiber, the sensitivity showed slight variations under the bending radii of infinite (flat), 5 cm and 1 cm at the same touching point (Fig. 2b and S11). Note that the multiply touching on single fiber cannot be distinguished, and the pressing stress is commonly used as an units for fiber-based sensor as the contact surfaces change under pressing due to the curving geometry of fiber surface [8,15]. With a small pressing stress of 0.07 N, the sensing fiber exhibited dramatically current change (Fig S11). The current response at low pressing stress mainly resulted from the increasing contact area between sheath and core electrodes, while the current response at high pressing stress was mainly attributed to the increasing contact area between CNT sheets in the CNT/PU composited sheath electrode and copper wire. In particular, the current changes exhibited good linearity within the range from 1 to 5 N (Fig. 2b) and can be further fitted into a linear formula related to applied force (Supporting Note 1.1). Under different bending states, the pressure sensitivity ($\Delta I/I_0$ per N) among this range is all around 1500 N^{-1}. Therefore, the sensing fiber can be applied on curved surfaces without the interference signal from bending stress. Besides, taking the advantage of the one-dimensional structure, its output currents were found to be nearly identical from different contact directions, regardless of bending curvatures (Fig S12). The cross-section images of X-ray micro-CT showed that the distances between copper and CNT electrodes were almost the same for different cross-sectional directions (Fig S13), which verified the stable performance for different contact directions. Such direction-independent property in sensing fiber distinguished it from those of typical planar devices, which can hardly detect accurate pressure unless a vertical stress was used. Due to the bending-independent property and one-dimensional fiber structure, the sensing fiber also exhibited twisting stability as its pressure sensitivity can be well maintained against up to 200 rad/meter twisting (Fig. 2c).

On the other hand, frequency responses of sensing fibers were examined to evaluate the responsiveness when bending radius was varied. The time-resolved measurement showed that the output signals kept intact and repeatable when the frequency increased from 0.5 Hz to 4 Hz. The response behavior between flat and bent devices exhibited negligible distinctions regardless of applied frequency, suggesting that the bending-independent perception can be well maintained under dynamic stimuli (Fig. 2d). The stability and durability of sensing fibers were also evaluated by cycling tests. The sensing fiber was bent to one certain curvature and applied with repeated loading-unloading pressure for over 100 cycles each time. Despite of the changes in bending radius, the output signals maintained stable without significant changes for over 400 cycles, which exhibited high reversibility and reproducibility under complex bending conditions (Fig. 2e).

Besides the feature of bending independence, the one-dimensional fiber enabled to recognize the touching position in the axial direction for improving reliability in spatial resolution. Based on a simplified single touching point model, the schematic

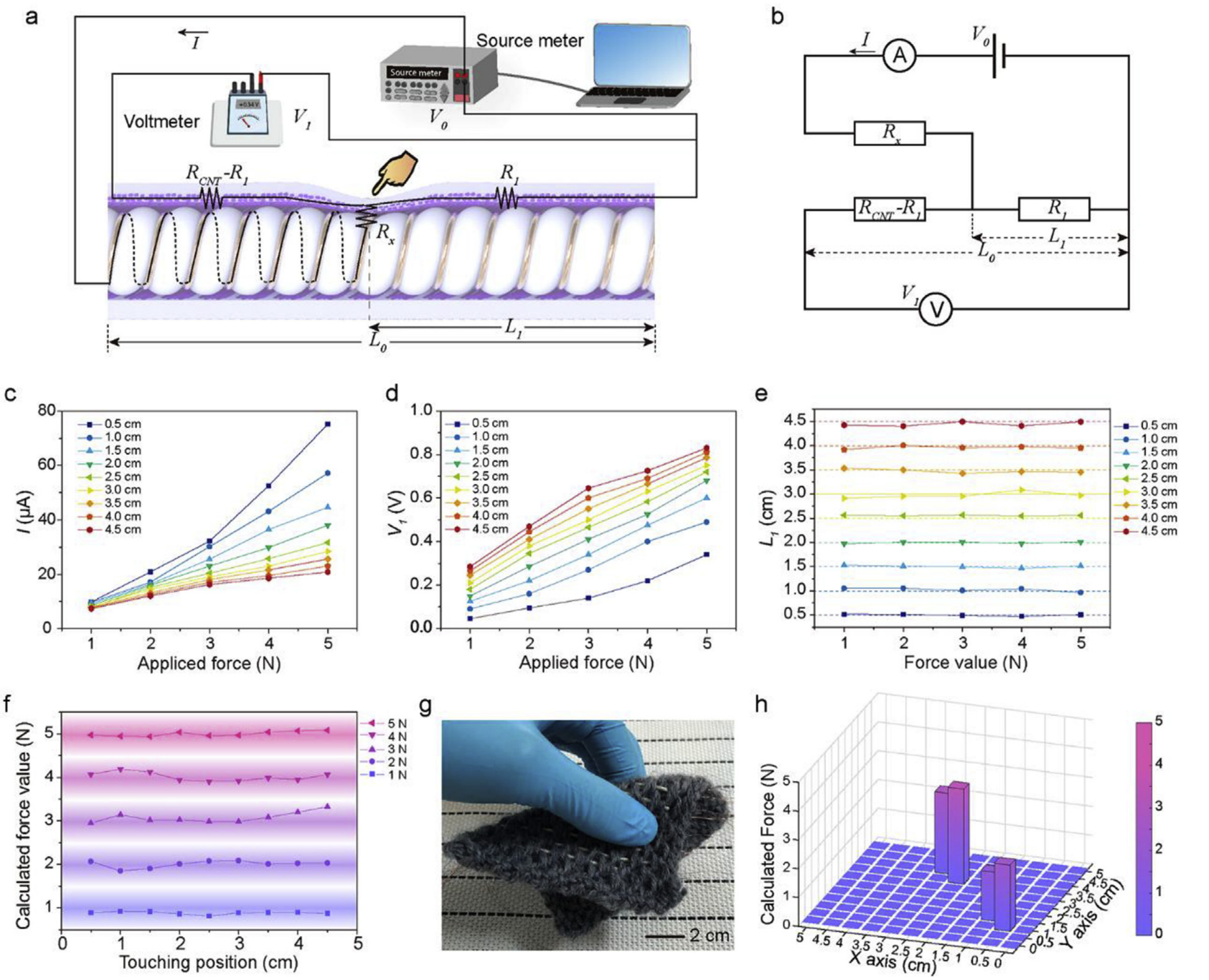

Fig. 3. | **Spatial acuity of TST. a**, Schematic illustration of the working principle and electric connections of a sensing fiber based on a simplified single touching point model. The value of R_1 is determined by the touching position (L_1) and R_x is the contact resistance depending on applied force (F). Source meter provides power source with a constant voltage (V_0) and measures the current value (I). A voltmeter records the divided voltage (V_1) of R_1. **b**, An equivalent electrical circuit diagram of the sensing fiber in **a**. **c**, Dependence of I on F at different L_1. **d**, Dependence of V_1 on F at different L_1. **e**, Dependence of the calculated L_1 based on the measured I and V_1 on real F. The dashed lines show the real contact positions. **f**, Dependence of the calculated F based on the measured I and V_1 on real L_1. The gradient areas show the deviation of calculated value from applied real forces. **g**, Optical image of a bent TST with two fingers applying pressure on it. **h**, Measured spatial distribution of pressure on the TST in **g**.

illustrations of the working principle and the corresponding equivalent electrical circuit were shown in Fig. 3a and 3b. The resistance of CNT/PU sheath electrode was divided into two sections by the touching point. The resistance of copper electrode and the connecting wires were much lower than CNT/PU electrode and can be negligible. The structure of the sensing fibers is similar to a slide rheostat. A source meter provided a constant voltage (V_0) and measured the current (I) while a voltmeter recorded the divided voltage (V_1) from the touching position to the right end (L_1) at the same time. Given the linear distribution of the resistance of the whole CNT/PU electrode (R_{CNT}) in the measured length of sensing fiber (L), L_1 can be represented by the following equation:

$$L_1 = \frac{V_1 \times L}{R_{CNT} \times I} \tag{1}$$

As shown in Fig. 3c and d, the values of I and V_1 were measured when the sensing fiber was loaded with different applied forces (F) from right to left every 5 mm. With the augment of L_1, the whole resistance in the circuit increased, leading to the decrease of I. The increased R_1 also induced the enhancement of divided voltage (V_1). Once the values of I and V_1 were measured, the touching position can be calculated by Equation (1). As the calculated L_1 was compared with the real touching position in Fig. 3e, slight deviations (<1 mm) were found between the calculated and the real values, verifying that the single touching point along the fiber can be recognized precisely.

On the other hand, the applied forces can also be figured out while simultaneously recognizing the touching position. Since the contact resistance between CNT/PU electrode and copper electrode (R_x) is determined by F, the value of F can be revealed in parameters correlated to R_x, namely I and V_1. Based on the measurement of V_1, resistance variation induced by touching position can be obtained and the value of F can be calculated by an equation only related to I and V_1 (Supporting Note 1.1). As shown in Fig. 3f, the calculated F closely matched the real applied forces. Therefore, the touching position in the axial direction of sensing fibers and the applied forces can be perceived by the specific measured values of I and V_1 accurately and simultaneously.

Bending-independent pressure perception and spatial acuity were well maintained after assembling sensing fibers into the TST. Through weaving sensing fibers in parallel, the location recognition was extended from one-dimensional axial direction to two-dimensional surface. When the sensing fabric was pinched by the two fingers into a folded shape, the applied forces and touching positions were successfully detected by the TST (Fig. 3g and h), without any interference from this extreme curvature. Considering that it is common for wearable fabrics to undergo complex deformations in real-time applications, the sensing fabric has great potential for practical pressure monitoring on skin surface.

The TST was also integrated with a glove to serve as a wearable tactile-sensing platform (Fig. 4). Five sensing fibers were integrated at the finger positions to evaluate pressure during human-environment interaction (Fig. 4a). The smart glove can detect and recognize physical contacts accurately under different gesticulations and motions in real time (Fig. 4a and b). When no pressure was loaded, the output currents remained at low level, regardless of the curvature of fingers, which were three to six orders of magnitude smaller than that of regular pressure responses. In contrast, the current increased drastically once the finger got in touch with objects, indicating that the smart glove can realize reliable and accurate pressure perception in curvilinear surfaces or dynamic movements. Thanks to the bending-insensitivity, interferences can be effectively avoided and reliable and accurate signals were provided. Therefore, such tactile-sensing platform shows promising applications in soft robotics with environmental recognition and perceptual prosthesis for disables.

At the back of hand in smart glove, a TST was assembled as well to function as a wearable digital control panel (Fig. 4c and d). The smart glove was connected with a data acquisition system (Fig S14). Analogue signals acquired by this system were quantified, filtered, analyzed and wirelessly transmitted to the mobile terminal. The output current (I) and divided voltage (V_1) of each sensor were simultaneously recorded in response to external pressure. The pressure intensity and contact position could be perceived and analyzed to map the tactile distribution. Based on the capability of

Fig. 4. | **Demonstration of the TST being integrated into a smart glove. a**, Optical images of a smart glove integrated with the TST on the five fingers, detecting physical contacts under different gesticulations, i.e., (i) open hand, (ii) pointing, (iii) touching, (iv) gripper and (v) grasping. **b**, The variation of current for each sensor on the glove during executing different gesticulations. **c-g**, Schematic illustration and optical images of a smart glove integrated with a TST on the back of hand and served as a user interface to control a cell phone.

locating touch points in fiber units, the TST can be divided into different function areas and each function area represented one certain digital signal (Fig. 4d). When pressure was applied to the smart glove by a user, the contact position could be quickly recognized and corresponding response would appear on the screen of mobile terminal. For example, a string of numbers was input in subsequence in the dialing software and a phone call was successfully made through this user interface (Fig. 4e–g and Supporting Movie 2). The textile-based sensing system effectively converted user instructions into machine operations and exhibited great potentials for achieving human-machine interface in the smart e-textile system.

Supplementary video related to this article can be found at https://doi.org/10.1016/j.carbon.2019.04.019.

4. Conclusions

In summary, we have demonstrated a TST by plain weaving novel sensing fibers with core-sheath structure. The sensing fiber and TST exhibited bending-independent pressure perception and spatial acuity in real time. Through introducing helically swollen architecture of core electrode in the sensing fibers, the TST can accurately detect pressures on different curved surfaces without the interference signal from bending stress. Such bending-independent response was highly stable and not disturbed by the contact direction and frequency of applied forces. Based on the resistance distribution in the core-sheath structure, touching position along the fiber and applied force can be perceived simultaneously. The TST can precisely map the surface pressure distribution even under folding. Furthermore, promising prototypes were shown by integrating TST into smart gloves for accurate tactile monitoring and wireless human-machine interaction. Therefore, the TST can provide an efficient route for reliable and accurate *in-situ* detection. This work also presents a new and general strategy in the advance of sensing materials and devices with high performances by designing core-sheath electrodes.

Acknowledgements

This work was supported by MOST (2016YFA0203302), NSFC (21634003, 51573027, 51673043, 21604012, 21805044, 21875042), STCSM (16JC1400702, 17QA1400400, 18QA1400700, 18QA1400800), SHMEC (2017-01-07-00-07-E00062) and Yanchang Petroleum Group.

Appendix A. Supplementary data

Supplementary data to this article can be found online at https://doi.org/10.1016/j.carbon.2019.04.019.

Conflict of interests

The authors declare no conflict of interests.

References

[1] G. Schwartz, B.C. Tee, J. Mei, A.L. Appleton, D.H. Kim, H. Wang, et al., Flexible polymer transistors with high pressure sensitivity for application in electronic skin and health monitoring, Nat. Commun. 4 (2013) 1859.

[2] Y. Gao, H. Ota, E.W. Schaler, K. Chen, A. Zhao, W. Gao, et al., Wearable microfluidic diaphragm pressure sensor for health and tactile touch monitoring, Adv. Mater. 29 (2017), 1701985.

[3] W. Yan, A. Page, T. Nguyen-Dang, Y. Qu, F. Sordo, L. Wei, et al., Advanced multimaterial electronic and optoelectronic fibers and textiles, Adv. Mater. 31 (2018), 1802348.

[4] C.M. Boutry, Y. Kaizawa, B.C. Schroeder, A. Chortos, A. Legrand, Z. Wang, et al., A stretchable and biodegradable strain and pressure sensor for orthopaedic application, Nat. Electron. 1 (2018) 314–321.

[5] C. Wan, G. Chen, Y. Fu, M. Wang, N. Matsuhisa, S. Pan, et al., An Artificial sensory neuron with tactile perceptual learning, Adv. Mater. 30 (2018), 1801291.

[6] M. Wang, W. Wang, W.R. Leow, C.J. Wan, G. Chen, Y. Zeng, et al., Enhancing the matrix addressing of flexible sensory arrays by a highly nonlinear threshold switch, Adv. Mater. 30 (2018), 1802516.

[7] S. Lee, A. Reuveny, J. Reeder, S. Lee, H. Jin, Q. Liu, et al., A transparent bending-insensitive pressure sensor, Nat. Nanotechnol. 11 (2016) 472–478.

[8] J. Ge, L. Sun, F.R. Zhang, Y. Zhang, L.A. Shi, H.Y. Zhao, et al., A stretchable electronic fabric artificial skin with pressure-, lateral strain-, and flexion-sensitive properties, Adv. Mater. 28 (2016) 722–728.

[9] B.W. Zhu, Z.Q. Niu, H. Wang, W.R. Leow, H. Wang, Y.G. Li, et al., Microstructured graphene arrays for highly sensitive flexible tactile sensors, Small 10 (2014) 3625–3631.

[10] S. Jung, J.H. Kim, J. Kim, S. Choi, J. Lee, I. Park, et al., Reverse-micelle-induced porous pressure-sensitive rubber for wearable human-machine interfaces, Adv. Mater. 26 (2014) 4825–4830.

[11] L. Wang, L. Wang, Y. Zhang, J. Pan, S. Li, X. Sun, et al., Weaving sensing fibers into electrochemical fabric for real-time health monitoring, Adv. Funct. Mater. 28 (2018), 1804456.

[12] J. Di, X. Zhang, Z. Yong, Y. Zhang, D. Li, R. Li, et al., Carbon-nanotube fibers for wearable devices and smart textiles, Adv. Mater. 28 (2016) 10529–10538.

[13] Y. Meng, Y. Zhao, C. Hu, H. Cheng, Y. Hu, Z. Zhang, et al., All-graphene core-sheath microfibers for all-solid-state, stretchable fibriform supercapacitors and wearable electronic textiles, Adv. Mater. 25 (2013) 2326–2331.

[14] Y. Liang, F. Zhao, Z.H. Cheng, Q.H. Zhou, H.B. Shao, L. Jiang, et al., Self-powered wearable graphene fiber for information expression, Nano Energy 32 (2017) 329–335.

[15] F. Zhao, Y. Zhao, H.H. Cheng, L.T. Qu, A graphene fibriform responsor for sensing heat, humidity, and mechanical changes, Angew. Chem. Int. Ed. 54 (2015) 14951–14955.

[16] N.Q. Luo, W.X. Dai, C.L. Li, Z.Q. Zhou, L.Y. Lu, C.C.Y. Poon, et al., Flexible piezoresistive sensor patch enabling ultralow power cuffless blood pressure measurement, Adv. Funct. Mater. 26 (2016) 1178–1187.

[17] L.T. Yu, J.C. Yeo, R.H. Soon, T. Yeo, H.H. Lee, C.T. Lim, Highly stretchable, weavable, and washable piezoresistive microfiber sensors, ACS Appl. Mater. Interfaces 10 (2018) 12773–12780.

[18] L. Viry, A. Levi, M. Totaro, A. Mondini, V. Mattoli, B. Mazzolai, et al., Flexible three-axial force sensor for soft and highly sensitive artificial touch, Adv. Mater. 26 (2014) 2659–2664.

[19] S. Takamatsu, T. Lonjaret, E. Ismailova, A. Masuda, T. Itoh, G.G. Malliaras, Wearable keyboard using conducting polymer electrodes on textiles, Adv. Mater. 28 (2016) 4485–4488.

[20] J. Lee, H. Kwon, J. Seo, S. Shin, J.H. Koo, C. Pang, et al., Conductive fiber-based ultrasensitive textile pressure sensor for wearable electronics, Adv. Mater. 27 (2015) 2433–2439.

[21] L. Persano, C. Dagdeviren, Y.W. Su, Y.H. Zhang, S. Girardo, D. Pisignano, et al., High performance piezoelectric devices based on aligned arrays of nanofibers of poly(vinylidenefluoride-co-trifluoroethylene), Nat. Commun. 4 (2013) 1633.

[22] X. Li, Z.H. Lin, G. Cheng, X. Wen, Y. Liu, S. Niu, et al., 3D fiber-based hybrid nanogenerator for energy harvesting and as a self-powered pressure sensor, ACS Nano 8 (2014) 10674–10681.

[23] W. Weng, P. Chen, S. He, X. Sun, H. Peng, Smart electronic textiles, Angew. Chem. Int. Ed. 55 (2016) 6140–6169.

[24] Y.C. Lai, J. Deng, R. Liu, Y.C. Hsiao, S.L. Zhang, W. Peng, et al., Actively perceiving and responsive soft robots enabled by self-powered, highly extensible, and highly sensitive triboelectric proximity- and pressure-sensing skins, Adv. Mater. 30 (2018), 1801114.

[25] Z. Liu, D. Qi, G. Hu, H. Wang, Y. Jiang, G. Chen, et al., Surface strain redistribution on structured microfibers to enhance sensitivity of fiber-shaped stretchable strain sensors, Adv. Mater. 30 (2018) 1704229.

[26] Y. Cheng, R. Wang, J. Sun, L. Gao, A Stretchable and highly sensitive graphene-based fiber for sensing tensile strain, bending, and torsion, Adv. Mater. 27 (2015) 7365–7371.

[27] M. Liu, X. Pu, C. Jiang, T. Liu, X. Huang, L. Chen, et al., Large-area all-textile pressure sensors for monitoring human motion and physiological signals, Adv. Mater. 29 (2017), 1703700.

[28] C. Pang, G. Lee, T. Kim, S.M. Kim, H.N. Kim, S. Ahn, et al., A flexible and highly sensitive strain-gauge sensor using reversible interlocking of nanofibres, Nat. Mater. 11 (2012) 795–801.

[29] X. You, J. He, N. Nan, X. Sun, K. Qi, Y. Zhou, et al., Stretchable capacitive fabric electronic skin woven by electrospun nanofiber coated yarns for detecting tactile and multimodal mechanical stimuli, J. Mater. Chem. C 6 (2018) 12981–12991.

[30] W. Zeng, L. Shu, Q. Li, S. Chen, F. Wang, X.M. Tao, Fiber-based wearable electronics: a review of materials, fabrication, devices, and applications, Adv. Mater. 26 (2014) 5310–5336.

[31] S.Y. Kim, S. Park, H.W. Park, D.H. Park, Y. Jeong, D.H. Kim, Highly sensitive and multimodal all-carbon skin sensors capable of simultaneously detecting tactile and biological stimuli, Adv. Mater. 27 (2015) 4178–4185.

[32] J. Deng, Y. Xu, S. He, P. Chen, L. Bao, Y. Hu, et al., Preparation of biomimetic hierarchically helical fiber actuators from carbon nanotubes, Nat. Protoc. 12 (2017) 1349–1358.

[33] J. Deng, J. Li, P. Chen, X. Fang, X. Sun, Y. Jiang, et al., Tunable photothermal actuators based on a pre-programmed aligned nanostructure, J. Am. Chem. Soc. 138 (2015) 225–230.
[34] A.R. Bunsell, Handbook of Tensile Properties of Textile and Technical Fibres, 2 nd ed, Elsevier, 2018.
[35] H. Liu, H. Zhao, S. Li, J. Hu, X. Zheng, R. Li, et al., Adhesion-free thin-film-like curvature sensors integrated on flexible and wearable electronics for monitoring bending of joints and various body gestures, Adv. Mater. Technol. (2018), 1800327.